Journal of Mining and Environment (JME), Vol. 15, No. 1, 2024, 73-96

Shahrood University of Technology

Journal of Mining and Environment (JME)

Journal homepage: www.jme.shahroodut.ac.ir

Iranian Society of Mining Engineering (IRSME)

Finite Element Analysis of Seismic Hazard in Post-mining Environments of Closed Underground Hard Rock Mines

Praveena Das Jennifer[1] and Porchelvan P.[2*]

1. Centre for Disaster Mitigation & Management (CDMM), Vellore Institute of Technology, Vellore, Tamil Nadu, India
2. School of Civil Engineering (SCE), Vellore Institute of Technology, Vellore, Tamil Nadu, India

Article Info

Received 5 August 2023
Received in Revised form 11 October 2023
Accepted 7 November 2023
Published online 7 November 2023

DOI: 10.22044/jme.2023.13445.2481

Keywords

Finite element method
Mine closure
Induced seismicity
Modelling studies
Dynamic modelling

Abstract

This paper presents a comprehensive study on the stability of the deep underground closed Kolar Gold Fields mine (3.2 km deep) under varying seismic loading conditions. The study utilized the Finite Element Method (FEM)-based Midas GTS NX software tool to conduct numerical simulations of seismic loads of varying intensities under multiple conditions of water level in the mine voids. The seismic loads applied were equivalent to the intensity of maximum mining-induced seismicity experienced in the mine. The study also examined the influence of the Mysore North Fault and its effects on the surface above the mining area. A seismic hazard vulnerability map of the mining area was developed based on the results for all simulated numerical model combinations. The results inferred that for a seismic load of PGA, 0.22 g, for fault and actual water level combination, very strong shaking and moderate potential surface damage were observed at vulnerable zones with a maximum PGA of 0.196 g and Peak Ground Velocity (PGV) of 0.49 m/s. The study highlights the importance of monitoring post-mining induced seismic activities using a dedicated microseismic monitoring system with sensors placed at the most vulnerable zone locations assessed from the numerical modelling studies carried out. Remedial measures suggested include regular dewatering of mine workings based on water accumulation and backfilling of mine voids with suitable fill material. The dynamic modelling approach using Midas GTS NX was found to be a more reliable, feasible, efficient, and simple method for assessing the stability of closed mines.

1. Introduction

Tectonic plate movements are primarily responsible for triggering earthquakes, which result in seismic events that can cause surface instability, damage to life, and property. While the concept of seismic events caused by tectonic plate movements is well-established, it's also important to note that human activities can induce seismic events [1]. Examples of human-induced seismicity include changes in water storage levels in dams or reservoirs [2, 3], hydraulic fracturing in the earth's subsurface or deeper layers [4], waste fluid disposal, oil and gas exploration activities [5, 6], construction work, blasting [7], and underground mining. The magnitude and duration of the seismicity induced in these cases can vary.

Underground mining presents unique challenges including maintaining excavation stability during drilling and blasting operations, managing shear slips, dealing with surface fracture formations, and preventing slope failures. Each mining excavation can lead to instability due to alterations in the stress state of the surrounding rock mass. This can build up stress, culminating in rockbursts in hard rock mines, and bumps in coal mines. These

✉ *Corresponding author: pporchelvan@vit.ac.in (Porchelvan p)*

rockbursts/bumps are the primary causes of mining-induced seismicity in mines. The understanding and analysis of mining-induced seismicity and its potential to cause seismic hazards within the mine and above the mining area remain unclear. Various researchers have proposed theories or concepts, and demonstrated the presence of mining-induced seismicity in active mines and even in closed or abandoned mines [8]. The damage to surface structures and underground mine structures is largely attributed to mining-induced seismicity. To evaluate the damaging effects, it's important to consider causal factors such as shear failure of rock mass, rockburst, pillar failures, and slip along fault lines, along with the magnitude of induced seismicity.

1.1. Mining-induced seismicity-worldwide

Seismicity induced by mining activities has been documented in various types of mines around the world including metalliferous mines, coal, gold, and potash mines. Specifically, this phenomenon has been observed in deep hard rock mines in several countries:

South Africa: Witwatersrand, Carletonville, and Klerksdorp mines [9, 10]

India: Kolar Gold Field mine [11]

Poland: Myslowic and Rudna mines [12, 13]

Canada: Elliot Lake Sudbury basin mine [14]

Sweden: Kiirunavaara and Kristineberg mines [15]

China: Metallic mines [16]

Australia: Mount Charlotte mine [17], Ridgeway mine [18], Beaconsfield mine [19] and Kalgoorlie district mines in Australia [20]

Sweden: Kiruna mine [21]

1.2. Post mining-induced seismicity-worldwide

According to a survey, around 50,000 abandoned mines were identified in Australia followed by the United States with around 22,000 mines, and Canada with 10,000 mines [22]. Even abandoned or closed mines can exhibit post-mining induced seismicity, posing potential risks to structures above them and nearby mined-out areas. These areas are classified as areas of grave concern. Post-mining induced seismicity has been reported in abandoned mines in Europe [22], South Africa [23], Sweden [24], Italy [25], Spain [26], and Japan [27].

1.3. Mining-induced seismicity hazard assessment

Numerous methods are used worldwide to assess the seismic risk associated with deep-level hard rock mining. These techniques, used in the evaluation of seismicity in deep mines, are based on parameters such as Excess Shear Stress (ESS) [28], Volume Excess Shear Stress (VESS) [29], Energy Release Rate (ERR) [30, 31], departure indexing (DI) [32], Local Energy Release Density (LERD) [33], Modeled Groundwork (MGW) - cell evaluation method [34], modified Mercalli intensity scale [35], Seismic Hazard Scale (SHS) [36], Coulomb stress change (ΔCFF) [37], Moment magnitude, seismic moment, and seismic energy - Modified Mercalli Intensity Scale (MMIS) [38], apparent stress [39].

Indirect waveform methods such as frequency content analysis and frequency-magnitude relations are also used in terms of the highest magnitude, Xmax, that has occurred during the monitoring time (T), the maximum seismic activity rate, λ, and the b value from Gutenberg-Richter [40]. Strong ground motion parameters – Peak Ground Acceleration (PGA) and Peak Ground Velocity (PGV) are also considered [41]. Seismic hazards can be examined either probabilistically or deterministically. The choice of assessment technique depends on the duration of the monitoring period (short, intermediate, or long-term), and each site will have specific requirements to achieve the objective.

All the methods mentioned above rely on data recorded by a dedicated network of seismic sensors. The analysis of this data yields source parameters such as event magnitude, time, depth, distance, frequency spectrum analysis, p-wave, s-wave, energy ratio, and stress drop. These parameters can assist in the seismic hazard analysis of the studied area. However, these methods are only applicable when the site is accessible, less prone to seismicity, has stable mining conditions, and is not flooded.

It's important to note the risks associated with inactive and closed mined-out sites. One of the main challenges with abandoned mines is the difficulty in conducting direct analyses to compute the geo-risks correlated with mined-out voids upon complete closure due to stability

issues and water ingress. There appear to be no specific guidelines or procedures for assessing the seismicity of an abandoned mine and its long-term risks. Post mining-induced seismic hazard and rock burst proneness could be evaluated by traditional fractal [42] and statistical analysis [43] of seismic data. Interpretation software and algorithms can be generated to understand the vibrations produced by seismic sources. Predicting mining seismic events using acoustic emission [44] methods.

The use of advanced techniques for data mining becomes essential when considering the inherent limits in conventional analytical approaches to solve problems related to rock mechanics and prediction utilizing numerical methods [45]. The organization and analysis of raw data in civil engineering have yielded valuable knowledge using numerous data mining techniques including statistical methods, regression tree (CART), case-based learning, symbolic learning, and artificial intelligence (AI) [46, 47, 48]. Artificial intelligence is the most widely utilized data mining technique in geotechnical and rock engineering. The short-term rockburst risk has recently been predicted using extreme gradient boosting (XGBoost), K-means clustering, and Catboost-based t-distributed stochastic neighbor embedding (t-SNE) techniques [49, 50, 51]. The limitation of the AI technique is the sample size and dataset distribution. The larger the dataset, the better and more reliable the output.

Ground motion parameters play a crucial role in studying the damaging effects, and can help quantify the intensity of damage and duration of the event. Using these parameters, areas can be classified as seismic vulnerable/non-vulnerable zones. The ground motion parameters used in this study for vulnerability assessment are Peak Ground Acceleration (PGA) and Peak Ground Velocity (PGV). Displacement (d) is another parameter that has been studied in the analysis.

PGA is the maximum ground acceleration recorded during a seismic event, and PGV is the maximum velocity recorded during a seismic event. These vibrations are detected by both vertical and horizontal sensors. PGA and PGV values are good indicators of damage caused, and for stronger events, PGA needs to be correlated with PGV. These parameters can vary greatly depending on factors like fault presence, depth and magnitude of the seismic event, duration of the event, and geology of the studied area. PGA and PGV are two major influencing parameters used to assess damage within a mine and on the surface above the mining area. Although displacement (d) is less commonly used as a ground motion measuring parameter, it's very useful for analysing surface structure instabilities when the studied area is subjected to seismic conditions.

1.4. Numerical modelling approach for seismic hazard assessment

There are numerous numerical modelling approaches available for seismic hazard assessment. These approaches are primarily categorized into continuous and discontinuous methods. The choice of one or more modelling approaches depends on the objective of the modelling. The decision to use a specific methodology is entirely dependent on the type of numerical model and the properties of the rock mass under investigation. Figure 1 presents the various numerical modelling approaches and their constitutive models.

Numerical modelling approaches	Numerical modelling methods	Constitutive models
Continuous	Finite Difference Method (FDM) Finite Element Method (FEM) Boundary Element method (BEM)	• Elastic (Hooke's law) • Plastic and elasto-plastic (e.g. Mohr-Coulomb, Hoek-Brown criteria) • Rock fractures models • Rheology effects (e.g. creep) • Dynamic loading (e.g. earthquakes) • Coupled thermo-hydro-mechanical models
Discontinuous	Discrete Element Method (DEM) Discrete Fracture Network (DFN)	
Hybrid continuous/discontinuous	Hybrid FEM/BEM Hybrid FEM/DEM Hybrid FDM/DEM	

Figure 1. Various modelling approaches and their constitutive models [52].

The numerical modelling technique chosen here is primarily to comprehend the response of the rock mass due to post-mining induced activity. The numerical modelling tool should be capable of handling both complex 3D geometry and larger scale models. Discontinuous models, which rely heavily on computation, are less suitable for large-scale models with fractured rock mass. For deep underground mines, the continuous modelling method will be implemented, focusing mainly on mining-induced stress and strain parameters. The continuous numerical modelling approach was chosen here due to the absence of precise information on the size, spatial distribution of voids, and orientation of geological features.

The Finite Element Method (FEM)-based numerical modelling software, Midas GTS NX, was chosen for several reasons. Firstly, FEM is a well-established and widely accepted method for solving complex structural and mechanical problems, including those encountered in mining engineering. It provides a robust and reliable approach to modelling the stress-strain behavior of geological materials under different loading conditions. Secondly, Midas GTS NX offers advanced capabilities for modelling complex geometries and boundary conditions, which are often encountered in mining applications. It also provides comprehensive analysis options for static, dynamic, and seismic loading conditions. This versatility makes it particularly suitable for the study conducted.

While other methods such as Finite Difference Method (FDM) or hybrid methods may also be suitable for certain applications, they may not offer the same level of flexibility and comprehensiveness as FEM-based software. For instance, FDM is typically more suited to regular geometries, and may not handle complex boundary conditions as effectively as FEM [53]. The Midas GTS NX software tool employs the FEM of partial differential equations to solve rock mechanics problems.

The numerical modelling studies shall be conducted step-by-step as follows:

- Collecting past-recorded seismic data (active mining and post-mining) of Kolar Gold fields mine
- Preparation of an integrated hydro-geomechanical model
- Dynamic analysis with site-specific ground motion parameters using FEM-based Midas GTS NX
- Identification of seismic vulnerable zones
- Estimation of seismic hazard

The conceptual framework for the numerical study is depicted in Figure 2.

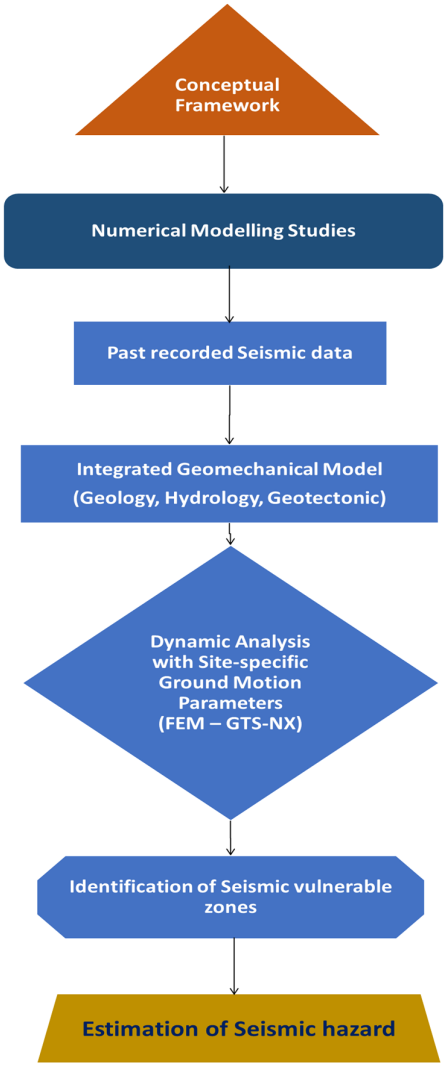

Figure 2. Conceptual framework for the numerical modelling studies.

2. Location

The studied area selected is the Kolar Gold fields mine in Karnataka, India. Once the second deepest mine in the world, the Kolar Gold field mine reached a mining depth of up to 3.2 km, and has a rich history of over 130 years of gold mining in India. Seismic activity induced by mining was reported both during active mining and after the mines were fully

closed in 2001 [54, 55]. As the mining area has been abandoned for more than two decades, there are significant risks associated with the mine including rock mass failure, support system failure, and water flooding into the mine voids. This study will focus on the seismic activity induced by mining that occurs in the closed mines of Kolar Gold fields. The approach involves using the FEM tool (Midas GTS NX) to assess the geotechnical seismic hazard associated with post-mine closure.

2.1. Geography

The abandoned underground Kolar Gold fields mine, a deep hard rock mine, is situated between latitudes 12.92^0 N to 12.98^0 N and longitudes 78.24^0 E to 78.27^0 E, at an altitude of 900 m above mean sea level. The mining area consists of three main mines: the Nundydroog Mine in the northern area, the Champion Reef mine in the central area, and the Mysore mine in the southern area. The Mysore North Fault is a significant fault that runs across the central mining area in a NW-SE direction. The Tennant Fault and Gifford Fault are two minor faults that run parallel to the main Mysore North Fault [54, 55]. A 3D representation of the entire mining area is depicted in Figure 3.

2.2. Geology of area

The Kolar Gold fields are located at the southernmost end of the Kolar schist belt, which is part of the greenstone Archean belt in Karnataka, southern India. The schist belt consists of two types of rock formations: the Dharwar schist, a metamorphosed basic igneous rock, and the peninsular gneiss, formed by granite intrusions from below. The schist belt extends approximately 80 km in a north-south direction, and spans a width of 3-4 km in an east-west direction[1-3]. The Kolar Gold fields mine contains seven gold-bearing lodes. The host rock for these gold-bearing lodes is the hornblende schist of Dharwar age, with pegmatites and gneisses. Auriferous quartz veins run in a north-south direction, almost parallel to the schist belt. The schist belt is faulted and folded with intrusions of pegmatite and dolerite porphyry dykes. At the surface, the fold dips at an angle of 30 degrees and follows a westerly dip at deeper levels within the mine [54, 55, 56].

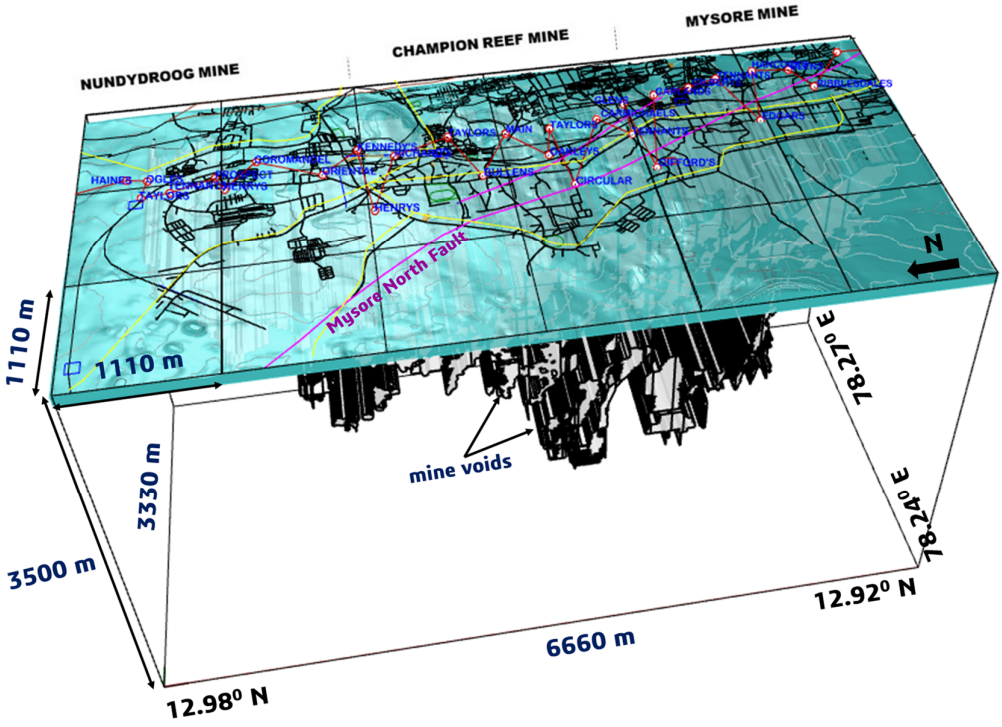

Figure 3. Kolar Gold fields mining area-3D view.

2.3. Mining method

The primary method of gold mining in the Kolar Gold fields mining area was the long hole open stoping method. Mining was conducted up to deeper levels with a vertical interval of 30 m between each level. As production reached deeper levels, the mining method was switched to a mechanized cut and fill method until the mines were completely closed. The mine voids are quite large and make up a significant portion of the ore body. After the ore body was excavated, the stopes were filled with cement/sand fill. In the final stages of mining, even the low-grade ore pillars were mined and rock waste was used as backfill material. Rock bolts were regularly used as a support system to stabilize the mining excavations, and grouted anchors were used in critical conditions and junctions. Cable bolting was also implemented for long-term stability of the underground mine, allowing for maximum production even at deeper levels [57].

3. Methodology

The entire mining area of 6.66 km (N-S) X 3.33 km (E-W) X 3.50 km (depth) is taken for this study (Figure 4). The area covers all the shafts of all three major mines of the mining region namely: Nundydroog mine (north), Champion Reef mine (central), and Mysore mine (south), stoped out areas constituting to about 70 percent of the mining area cover about 1400 km of tunnel work. The model is considered the deepest champion reef mine, which has reached a mining depth of 113 level (3.2 km deep) [57, 58]. The 3D model was developed taking the major Mysore North Fault traversing across the mining area with the dumps and mine voids (Figure 3). The lithological details were taken from the geological plan-Kolar Gold Fields (survey department 1956). The 3D geological model is shown in Figure 5.

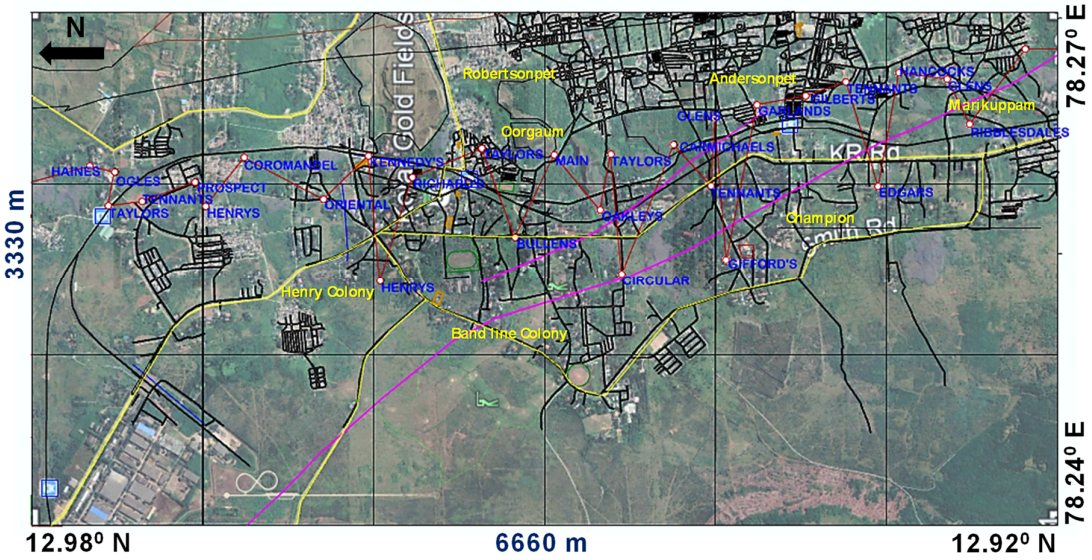

Figure 4. Kolar Gold fields entire mining area considered for analysis [57].

3.1. Numerical model

The stability analysis of the entire mining area was conducted using a model based on the Generalized Hoek-Brown constitutive continuum behavior, subjecting the model to various seismic loads. The non-linear Generalized Hoek-Brown criterion [59] was employed to derive the rock mass input data necessary for analyses involving excavations in underground hard rock. The physico-mechanical properties of the material, shown in Table 1, were used as inputs in the model. These include uniaxial compressive strength, elastic modulus, unit weight, and triaxial properties such as cohesion and friction angle. The property values of the geological materials at the Kolar Gold fields mine location, tested in the laboratory, were obtained from the Geological Survey of India (GSI) report [58]. Based on these laboratory test results, Hoek and Brown intact rock parameters and GSI parameters were used. The criterion was applied

to define the Hoek-Brown material constant (mi), unconfined compressive strength (UCS), and Geological Strength Index (GSI) for each geology based on rock mass structure, type, and discontinuity. The geomechanical properties of intact rock, namely mi, UCS, and GSI were used to calculate m and s (Hoek-Brown constants) using the empirical relations [59] below:

$$s = \exp\left(\frac{(GSI - 100)}{9}\right)$$

$$m = mi \exp\left(\frac{(GSI - 100)}{28}\right)$$

Table 1 presents the elastic non-linear properties that were used as inputs in the model. Water is modelled as a linear continuum material with a Poisson's ratio of 0.49. The model employs Rayleigh's damping approach. Prior to executing the non-linear time history analysis, an eigenvalue analysis was conducted to identify the percentage of mass participation and to obtain both f1 and f2 frequencies required for running the model.

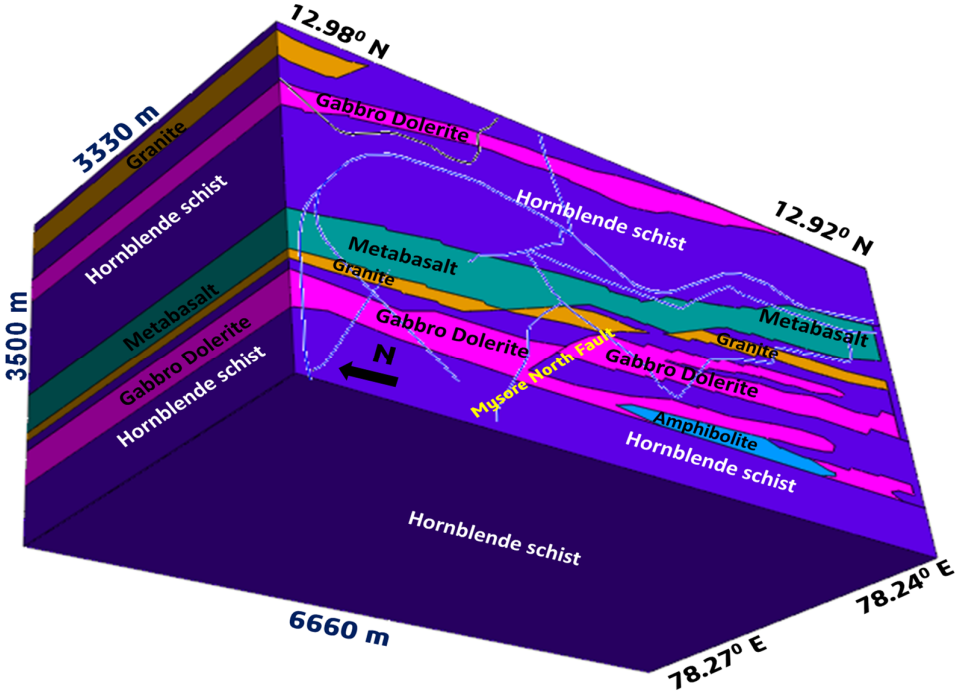

Figure 5. 3D Geological model of the entire mining area (studied area) [57].

Table 1. Physico-mechanical properties of the lithological units taken as inputs in model [57].

Material properties	Gabbro Dolerite	Amphibolite	Granite	Meta Basalt	Hornblende Schist
Elastic Modulus x 10^7 (kN/m^2)	8.54	8.40	6.82	9.36	8.26
Unit Weight (kN/m^3)	28.63	29.40	26.68	29.61	29.62
GSI	40	40	45	40	30
Intact Rock Parameter	7	25	30	17	4
Disturbance Factor	0.8	0.8	0.8	0.8	0.8
mb	0.196810	0.702891	1.135860	0.477966	0.062015
s	0.000113	0.000113	0.000240	0.000113	0.0000248
a	0.511368	0.511368	0.508086	0.511368	0.522344
Uniaxial Compressive Strength (kN/m^2)	87377	196133	166713	294200	152199
Damping Ratio	0.05	0.05	0.05	0.05	0.05

3.2. Dynamic Seismic load

The artificial earthquake generator technique [60] was utilized to simulate the seismic load, with the maximum expected response derived from the design power spectral density of the area. An eigenvalue analysis was conducted to achieve a similar target spectrum. The design spectrum of the studied area was taken in accordance with IS 1893 (2002). The artificial earthquake was simulated using the Peak Ground Acceleration (PGA) of the seismic event with the highest magnitude recorded in the mining area to date [61]. The acceleration time histories were plotted according to the response spectrum of Kolar Gold fields [57] (Figure 6). The PGAs chosen for the study were based on the least magnitude event value (Case A = 0.06 g), an intermediate value (Case B = 0.10 g), and the highest magnitude event value (Case C = 0.22 g). These values were derived from data reported in previous seismic studies conducted in the Kolar Gold fields area.

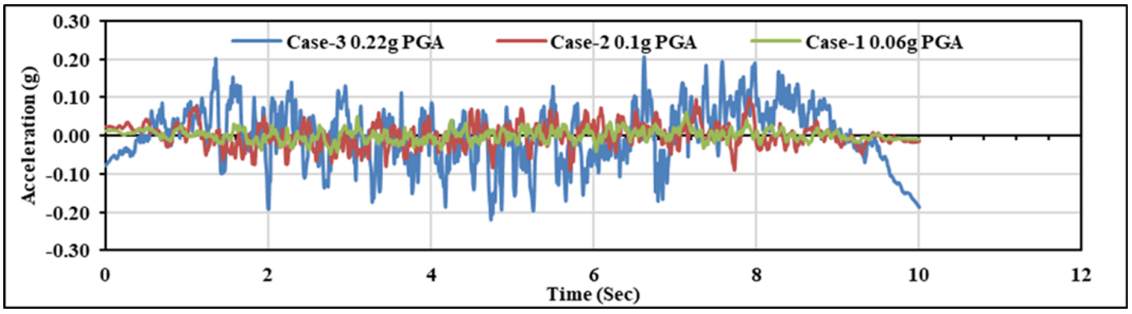

Figure 6. Acceleration time history plot for PGA - 0.06 g, 0.10 g, and 0.22 g [57].

4. Analysis and Results

A parametric seismic-nonlinear time history analysis was conducted for six combination case conditions, based on the presence or absence of a fault and the presence or absence of water in the mine voids. These six case conditions were further analyzed for all three cases of varying Peak Ground Accelerations (PGA): Case A (0.06 g), Case B (0.10 g), and Case C (0.22 g). The different PGAs of 0.06 g (Case A), 0.10 g (Case B), and 0.22 g (Case C) were applied as ground acceleration at the bottom of the model along the x-direction. The parameters varied in the analysis include Peak Ground Acceleration (PGA) - seismic load applied in the x-direction, water level, and presence of a fault. The case conditions with the various combinations analyzed are presented in Table 2.

Table 2. The six case conditions with various combinations used for the model studies.

Case No.	Condition	Fault	Water level (m)	(PGA)-seismic load applied
Case 1	No fault and no water	Absent	No water	0.06 g
				0.10 g
				0.22 g
Case 2	No fault and water	Absent	Up to 500 m from surface	0.06 g
				0.10 g
				0.22 g
Case 3	No fault and full water	Absent	Up to ground level	0.06 g
				0.10 g
				0.22 g
Case 4	Fault and no water	Present	No water	0.06 g
				0.10 g
				0.22 g
Case 5	Fault and water	Present	Up to 500 m from surface	0.06 g
				0.10 g
				0.22 g
Case 6	Fault and full water	Present	Up to ground level	0.06 g
				0.10 g
				0.22 g

A total of 18 models were run for the six case conditions under three peak ground accelerations (PGA) of 0.06 g (Case A), 0.10 g (Case B), and 0.22 g (Case C) for all the above case combinations. The results obtained for these combinations are presented with the presence of a fault as a primary parameter for comparison. The model results for the different conditions will be presented together to facilitate a more comprehensive analysis.

Condition 1: Absence of water (Case 1 and Case 4)

This condition examines the impact of the presence or absence of the major Mysore North Fault (MNF). The results for Peak Ground Accelerations (PGA) and displacements (d) observed at the surface for 0.06 g (Case A), 0.10 g (Case B), and 0.22 g (Case C) applied as ground acceleration equivalent to that of a seismic load of an earthquake of the same magnitude at the bottom of the model along the x-direction are presented in Figure 7.

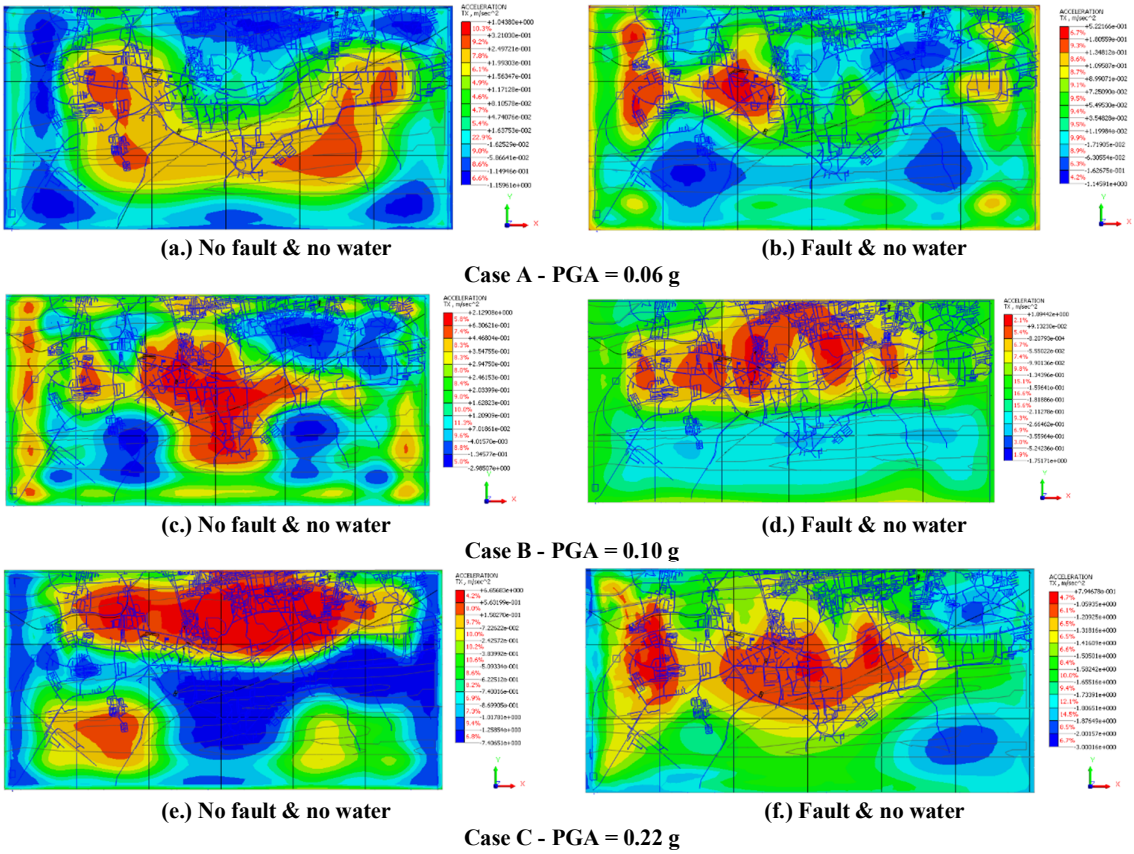

(a.) No fault & no water **(b.) Fault & no water**

Case A - PGA = 0.06 g

(c.) No fault & no water **(d.) Fault & no water**

Case B - PGA = 0.10 g

(e.) No fault & no water **(f.) Fault & no water**

Case C - PGA = 0.22 g

Figure 7. Peak Ground Accelerations observed at the surface for Condition 1 (a.) to (f.).

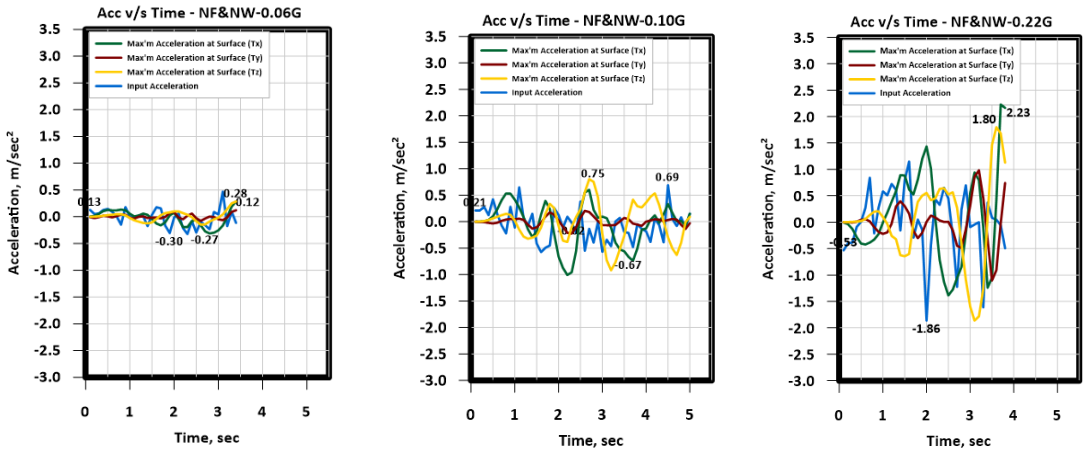

(a.) Case A - PGA = 0.06 g (b.) Case B - PGA = 0.10 g (c.) Case C - PGA = 0.22 g

Figure 8. Acceleration time history plot - at the ground surface for all three cases (NF & NW).

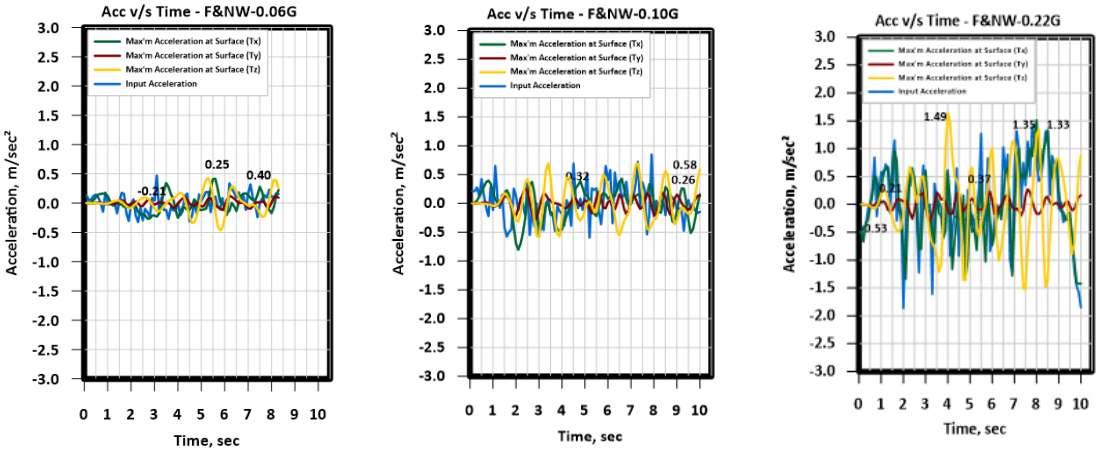

(a.) Case A - PGA = 0.06 g (b.) Case B - PGA = 0.10 g (c.) Case C - PGA = 0.22 g

Figure 9. Acceleration time history plot - at the ground surface for all three cases (F & NW).

As seen in Figure 7, the presence of the fault significantly influences the seismic loads, especially when there is no water within the mining area. The following observations can be made for Case A, Case B, and Case C:

For Case A (PGA = 0.06 g) - without a fault, the maximum PGA is 0.321 m/s². The central and mostly non-inhabited areas are affected by this seismic load.

For Case A (PGA = 0.06 g) - with a fault, the maximum PGA is 0.522 m/s². The northern central parts and mostly less inhabited areas are affected by this seismic load. The inhabited area of Henry's colony shows a maximum PGA of 0.180 m/s².

For Case B (PGA = 0.10 g) - without a fault, the maximum PGA is 2.129 m/s². The areas affected by this seismic load are the central part and mostly the Band line colony and Oorgaum station surrounding areas. The inhabited area of the Band line colony shows a maximum PGA of 0.630 m/s².

For Case B (PGA = 0.10 g) - with a fault, the maximum PGA is 1.89 m/s². The central parts of Oorgaum, parts of Andersonpet and surrounding areas are affected by this seismic load.

For Case C (PGA =0.22 g) - without a fault, the maximum PGA is 6.65 m/s². Major parts of Oorgaum, some parts of Andersonpet and some parts of Robertsonpet areas are affected by this seismic load. The less inhabited area of Henry's colony shows a maximum PGA of 0.56 m/s².

For Case C (PGA = 0.22 g) - with a fault, the maximum PGA is 0.795 m/s². The less inhabited areas of Oorgaum and surrounding areas are affected by this seismic load.

The Acceleration time history plots at the ground surface for all three cases for condition

1 without fault are shown in Figure 8, and with the presence of the fault in Figure 9.

The spatial distribution of maximum shear stress for condition 1 for all three cases showing the influence of the presence of fault is shown in Figure 10.

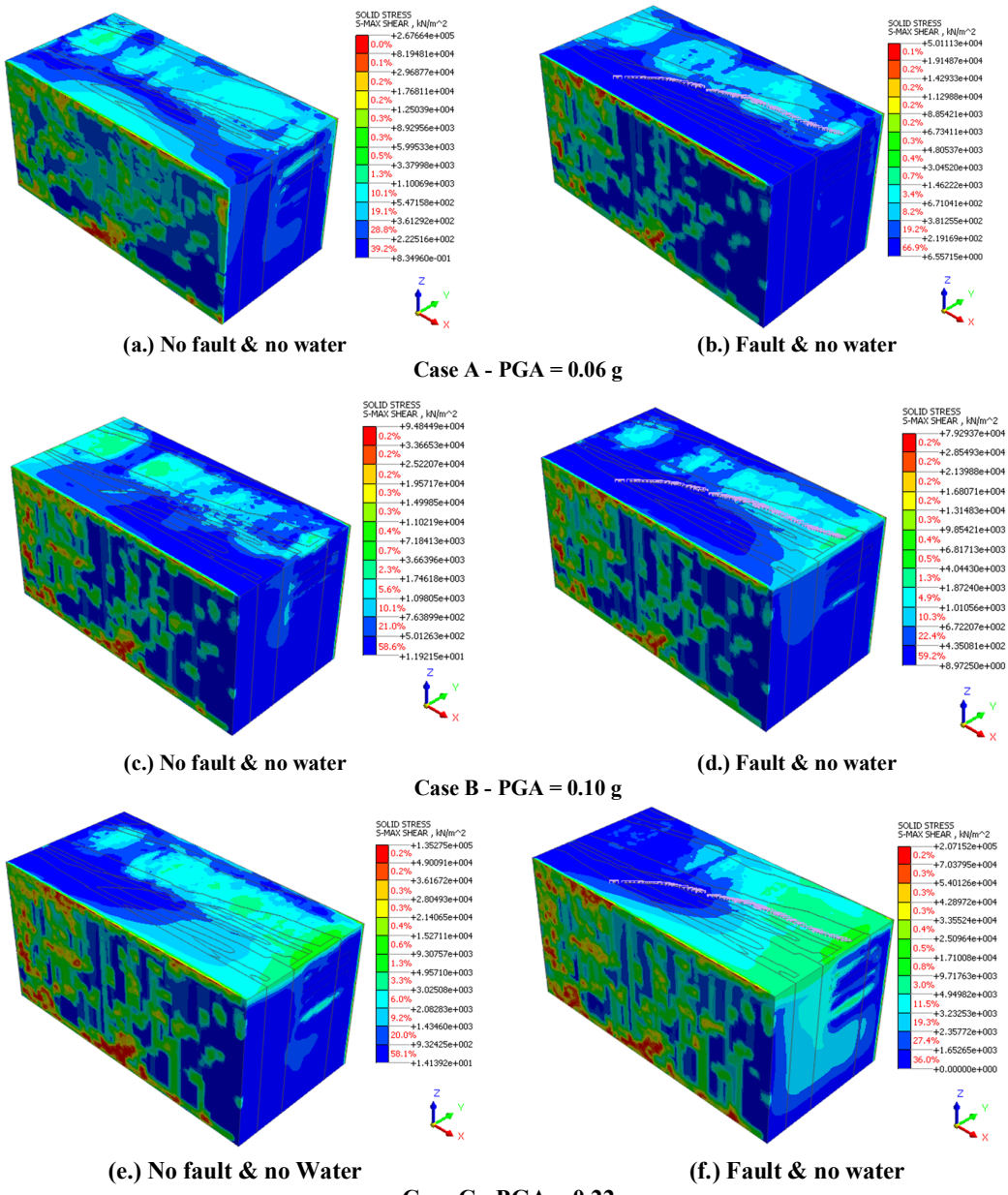

(a.) No fault & no water **(b.) Fault & no water**

Case A - PGA = 0.06 g

(c.) No fault & no water **(d.) Fault & no water**

Case B - PGA = 0.10 g

(e.) No fault & no Water **(f.) Fault & no water**

Case C - PGA = 0.22 g

Figure 10. Spatial distribution of maximum shear stress for condition 1 (a.) to (f.).

Condition 2: Presence of water upto 500 m from the surface (Case 2 and Case 5)

This condition examines the impact of the presence or absence of the major Mysore North Fault (MNF) when water is present up to 500 m from the surface. The results for Peak Ground Accelerations (PGA) and displacements (d) observed at the surface for 0.06 g (Case A), 0.10g (Case B), and 0.22 g (Case C) applied as ground acceleration equivalent to that of a seismic load of an earthquake of the same magnitude at the bottom of the model along the x-direction are presented in Figure 11.

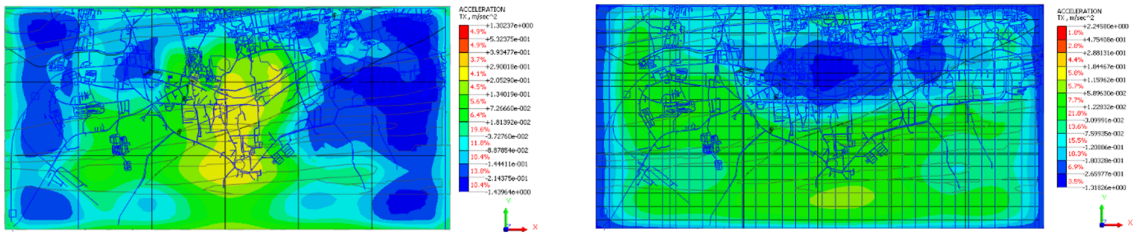

(a.) No fault & water (b.) Fault & water

Case A - PGA = 0.06 g

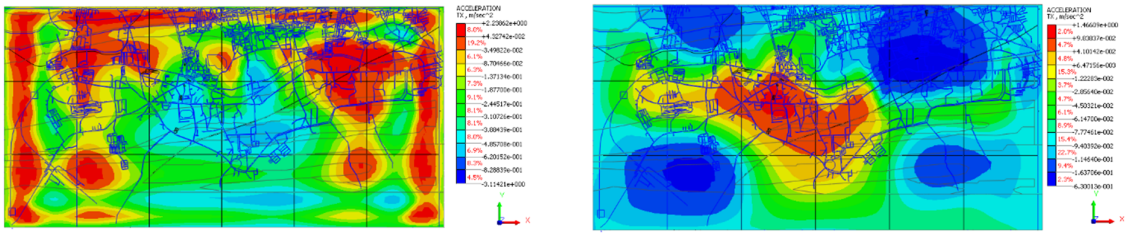

(c.) No fault & water (d.) Fault & water

Case B - PGA = 0.10 g

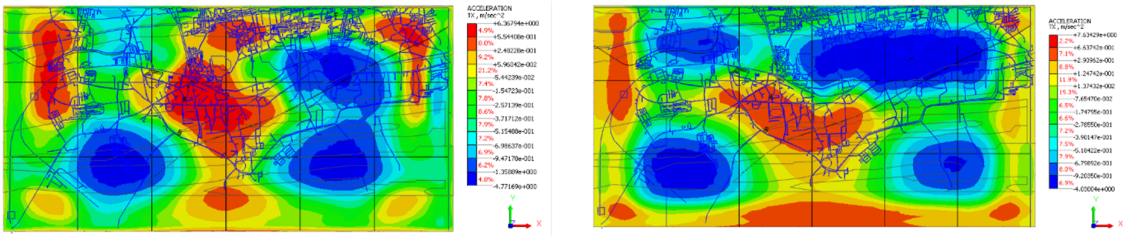

(e.) No fault & water (f.) Fault & water

Case C - PGA = 0.22 g

Figure 11. Peak ground accelerations observed at the surface for condition 2 (a.) to (f.).

As seen in Figure 11, the presence of the fault significantly influences the seismic loads, especially when water is present up to 500 m from the surface of the mine. The following observations can be made for Case A, Case B, and Case C:

For Case A (PGA = 0.06 g) - without a fault, the maximum PGA is 0.393 m/s². The central part and mainly band line colony areas are affected by this seismic load. The less inhabited area of the band line colony shows a maximum PGA of 0.290 m/s².

For Case A (PGA = 0.06 g) - with a fault, the maximum PGA is 0.184 m/s². The less inhabited areas near the band Line colony are affected by this seismic load.

For Case B (PGA = 0.10g) - without a fault, the maximum PGA is 2.298 m/s². The areas affected by this seismic load are Champion, Andersonpet, Marikuppam, parts of Henry's colony and surrounding areas.

For Case B (PGA = 0.10g) - with a fault, the maximum PGA is 1.466 m/s². The central parts of Oorgaum, covering the station and surrounding areas are affected by this seismic load. The inhabited area of Oorgaum shows a maximum PGA of 0.0983 m/s².

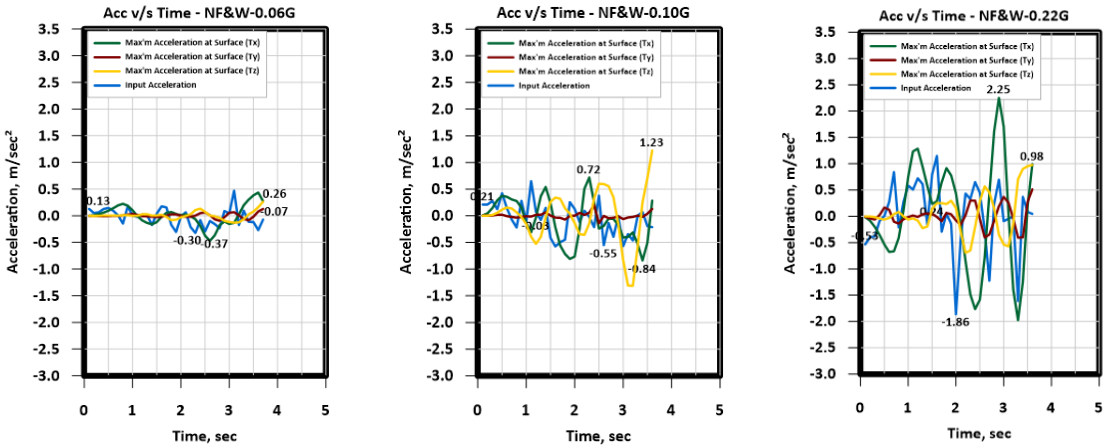

(a.) Case A - PGA = 0.06g (b.) Case B - PGA = 0.10g (c.) Case C - PGA = 0.22g

Figure 12. Acceleration time history plot - at the ground surface for all three cases (NF & W).

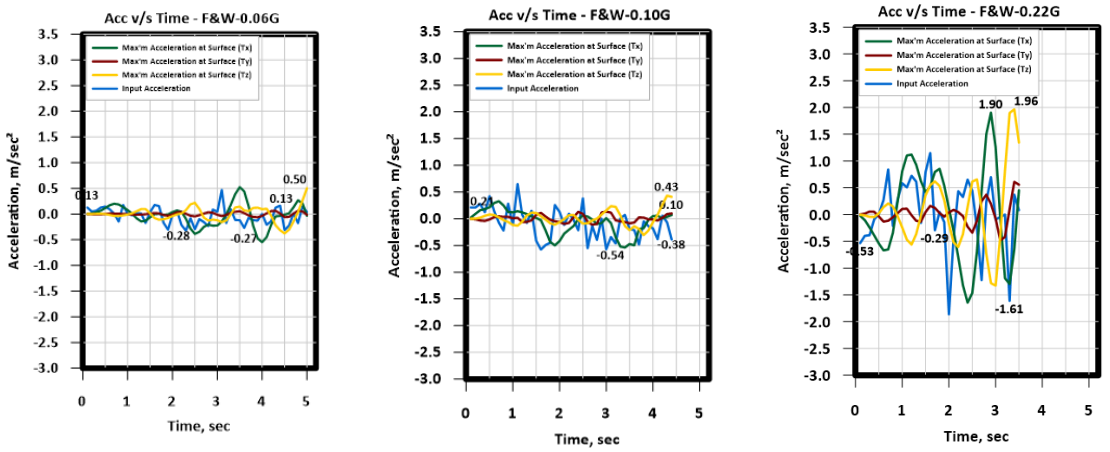

(a.) Case A - PGA = 0.06 g (b.) Case B - PGA = 0.10 g (c.) Case C - PGA = 0.22 g

Figure 13. Acceleration time history plot - at the ground surface for all three cases (F & W).

For Case C (PGA = 0.22 g) - without a fault, the maximum PGA is 6.36 m/s². Major parts of Oorgaum, some parts of Andersonpet, and some parts of Robertsonpet areas are affected by this seismic load. The less inhabited area behind Henry's colony shows a maximum PGA of 0.554 m/s².

For Case C (PGA=0.22 g) - with a fault, the maximum PGA is 7.63 m/s². The less inhabited areas of Oorgaum are affected by this seismic load.

The Acceleration time history plots at the ground surface for all three cases for condition 2 without fault are shown in Figure 12, and with the presence of the fault in Figure 13.

The spatial distribution of maximum shear stress for condition 2 for all three cases showing the influence of the presence of fault is shown in Figure 14.

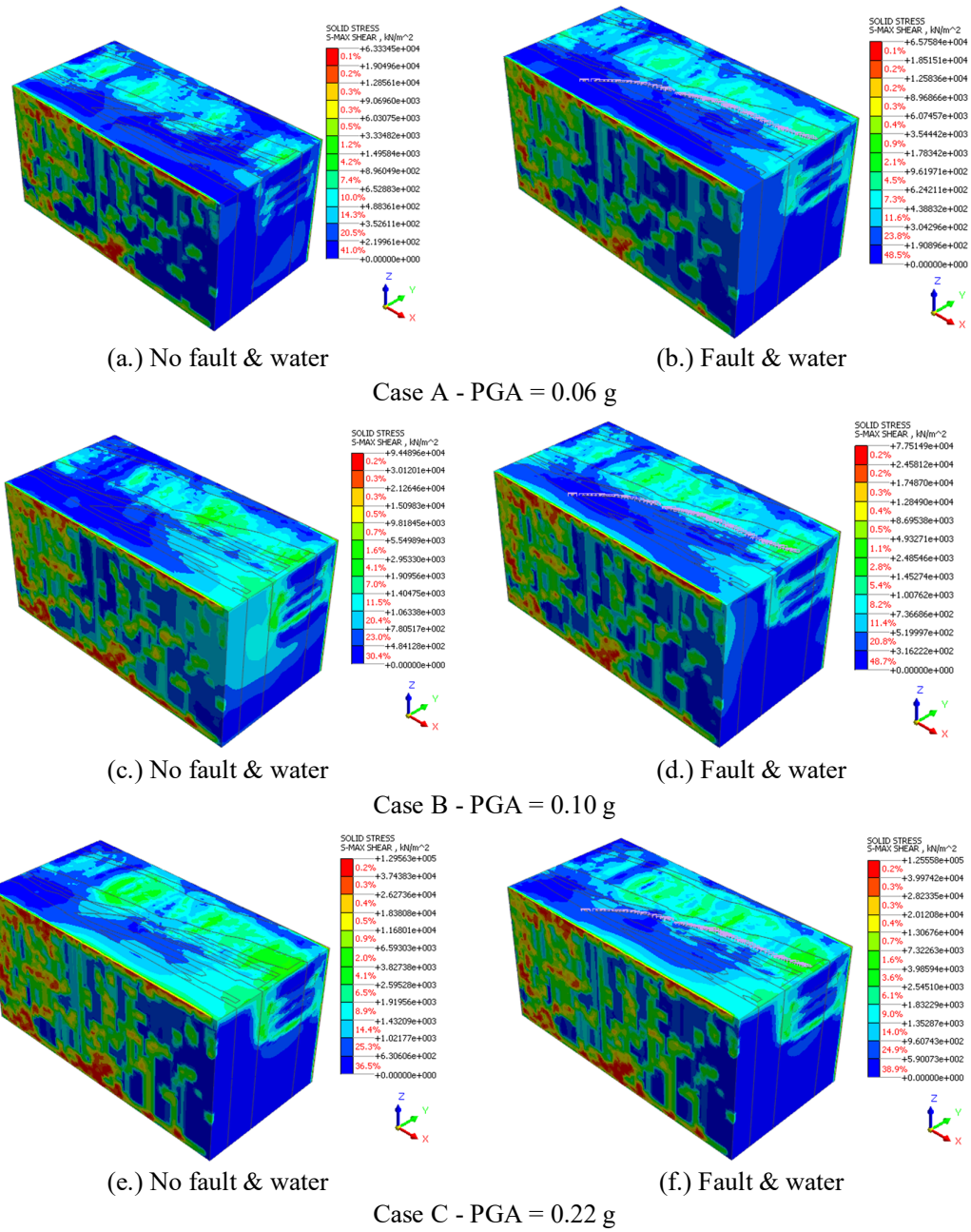

(a.) No fault & water (b.) Fault & water

Case A - PGA = 0.06 g

(c.) No fault & water (d.) Fault & water

Case B - PGA = 0.10 g

(e.) No fault & water (f.) Fault & water

Case C - PGA = 0.22 g

Figure 14. Spatial distribution of maximum shear stress for condition 2 (a.) to (f.).

Condition 3: Presence of water upto surface (Case 3 and Case 6)

This scenario is examined to understand the impact of the presence or absence of the significant Mysore North Fault (MNF). The outcomes of the Peak Ground Accelerations (PGA) and displacements (d) recorded at the surface for 0.06 g (Case A), 0.10 g (Case B), and 0.22 g (Case C) are presented in Figure 15. These values are applied as ground acceleration, equivalent to a seismic load of an earthquake of the same magnitude at the base of the model in the x-direction.

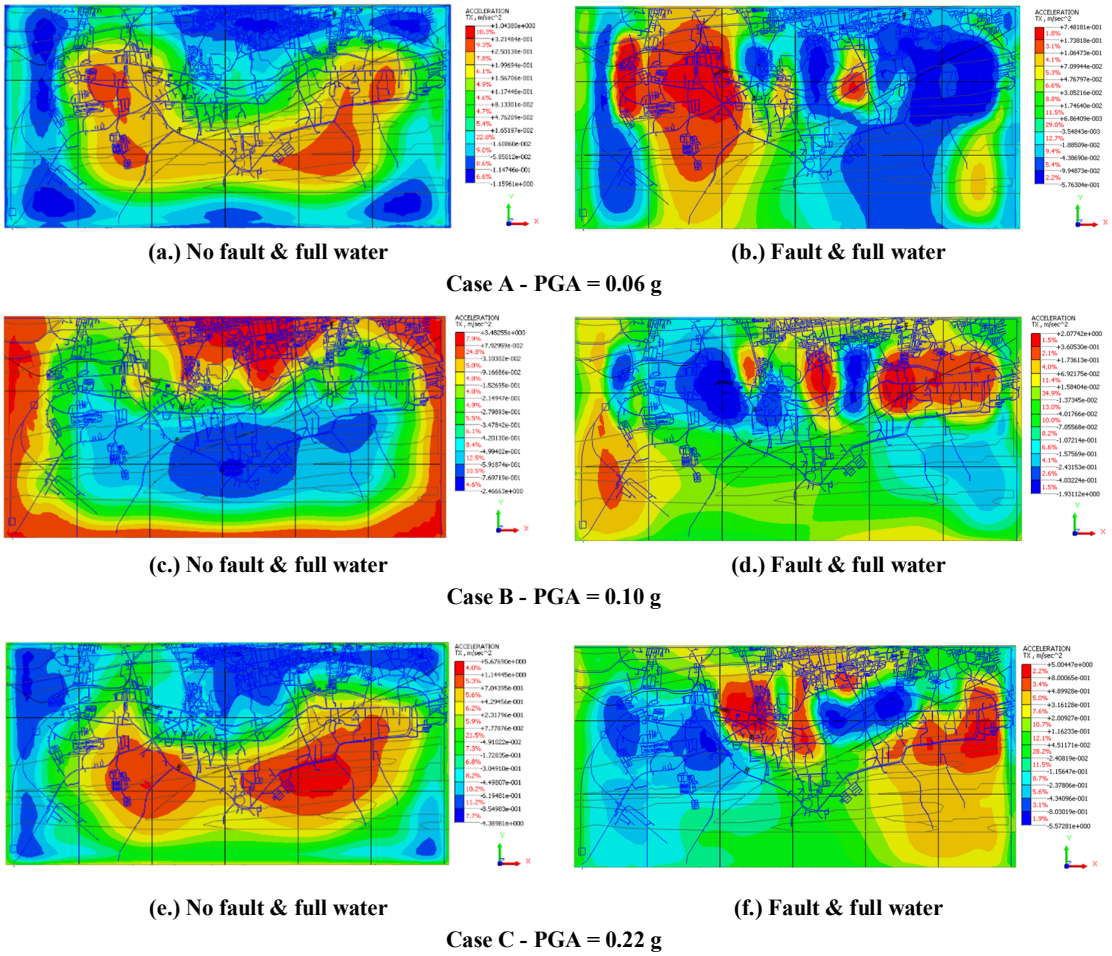

(a.) No fault & full water **(b.) Fault & full water**

Case A - PGA = 0.06 g

(c.) No fault & full water **(d.) Fault & full water**

Case B - PGA = 0.10 g

(e.) No fault & full water **(f.) Fault & full water**

Case C - PGA = 0.22 g

Figure 15. Peak ground accelerations observed at the surface for condition 3 (a.) to (f.).

From Figure 15, it's evident that the fault has a significant impact when subjected to varying seismic loads and considering a condition where water fills the mining area. Observations for Case A, Case B, and Case C are as follows:

For Case A (PGA = 0.06 g) - in the absence of a fault, the highest PGA is 0.321 m/s². The seismic load affects areas such as Henry's colony, parts of Champion, and nearby regions. The populated area of Henry's colony exhibits a maximum PGA of 0.250 m/s².

For Case A (PGA = 0.06 g) - in the presence of a fault, the highest PGA is 0.748 m/s². The seismic load affects areas such as Henry's colony, parts of Oorgaum, and nearby regions.

For Case B (PGA = 0.10 g) - without a fault, the highest PGA is 3.482 m/s². The seismic load affects areas such as Robertsonpet, some parts of Andersonpet, and Marikuppam regions. The less populated area exhibits a maximum PGA of 0.079 m/s².

For Case B (PGA = 0.10 g) - with a fault, the highest PGA is 2.077 m/s². The seismic load affects central parts of Champion and Andersonpet, and some parts of Oorgaum. The less populated area exhibits a maximum PGA of 0.360 m/s².

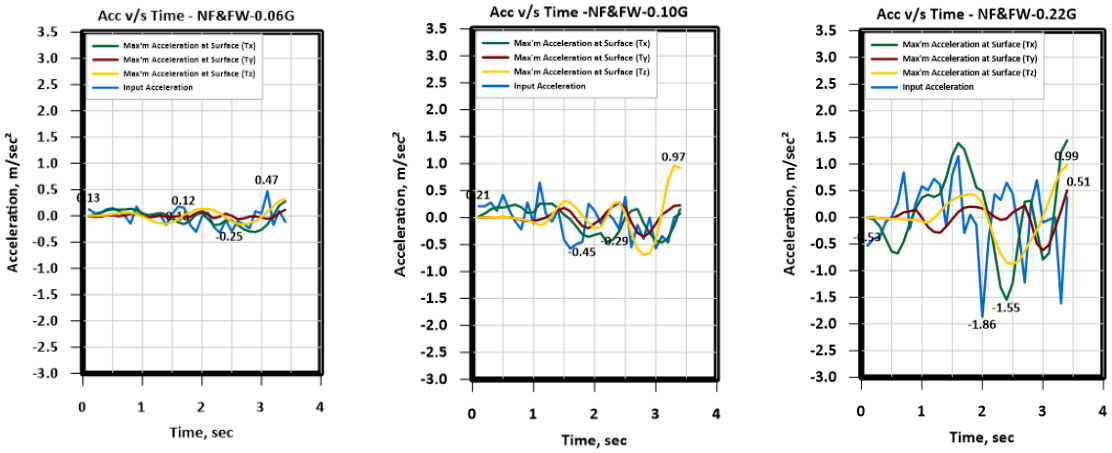

(a.) Case A - PGA = 0.06 g (b.) Case B - PGA = 0.10 g (c.) Case C - PGA = 0.22 g

FW).

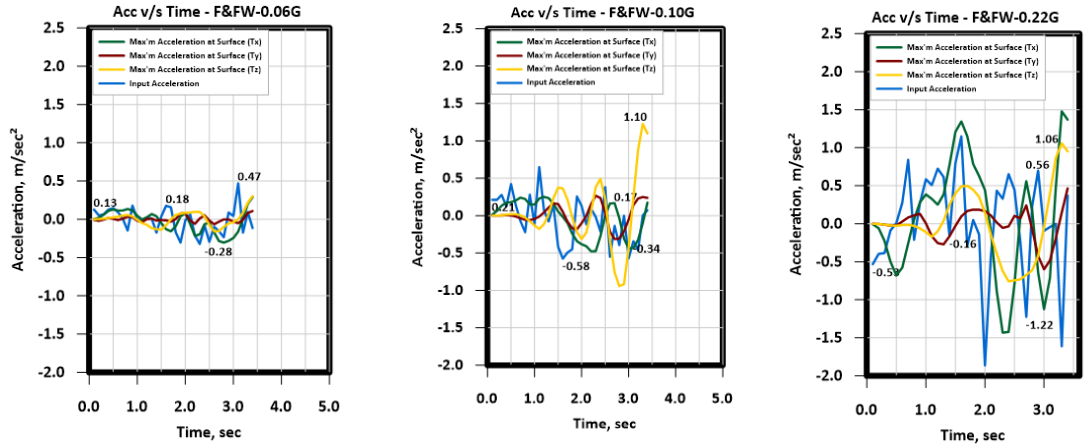

(a.) Case A - PGA = 0.06 g (b.) Case B - PGA = 0.10 g (c.) Case C - PGA = 0.22 g

Figure 17. Acceleration time history plot - at the ground surface for all three cases (F & FW).

For Case C (PGA = 0.22 g) - without a fault, the highest PGA is 5.676 m/s². The seismic load affects areas such as Henry's colony, band line colony, and some parts of Champion. The less populated area exhibits a maximum PGA of 1.144 m/s².

For Case C (PGA = 0.22 g) - with a fault, the highest PGA is 5.00 m/s². The seismic load affects inhabited areas of Oorgaum, Marikuppam, and surrounding regions. The less populated areas exhibit a maximum PGA of 0.800 m/s².

The Acceleration time history plots for all three cases for condition 3 without fault are depicted in Figure 16, and with the presence of the fault in Figure 17.

Figure 18 shows the spatial distribution of maximum shear stress for condition 3 for all three cases, highlighting the influence of the presence of fault.

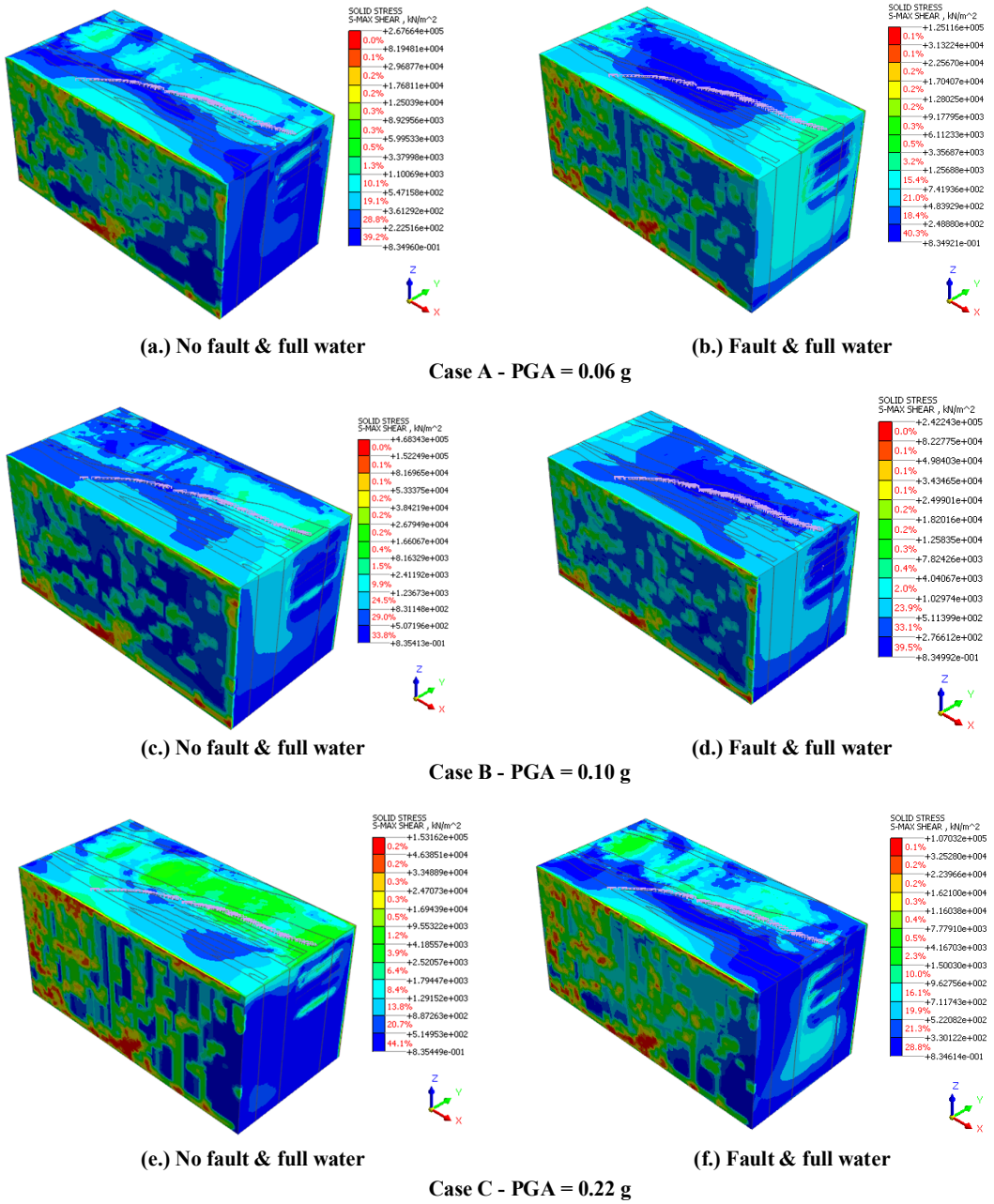

Figure 18. Spatial distribution of maximum shear stress for condition 3 (a.) to (f.).

5. Discussion

As per the seismic zoning map of India, Kolar Gold fields is situated in Zone II, which is identified as the least seismically active zone. The classification of the zone clearly indicates that the mining region is not susceptible to significant earthquakes. The mining area is largely unaffected by tectonic stresses, and the alteration in stress state within and around the rock mass, leading to instability within the mine, is primarily due to post-mining induced seismicity. Given that a major fault line runs directly through the mining area, it's crucial to factor in the presence of this fault in all analyses. Only considering cases with the presence of a fault, the acceleration, velocity, and displacement time plots at the ground surface for all three cases are analyzed and depicted in Figures 19, 20, and 21. The maximum PGA, PGV, and displacements for Cases 4 to 6 (cases with a fault) are presented in Table 3.

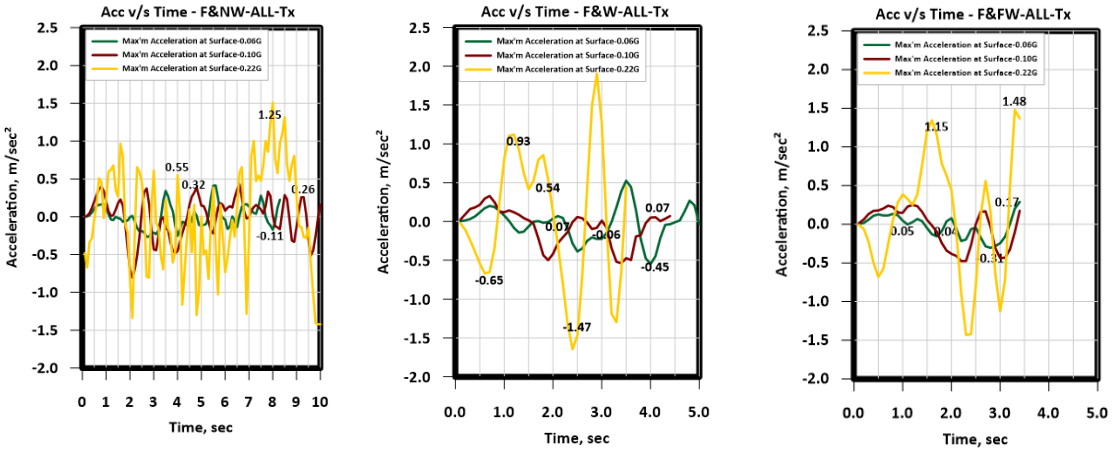

(a.) Fault & no water (b.) Fault & water (c.) Fault & full water

Figure 19. Acceleration time history plot - at the ground surface for all three cases.

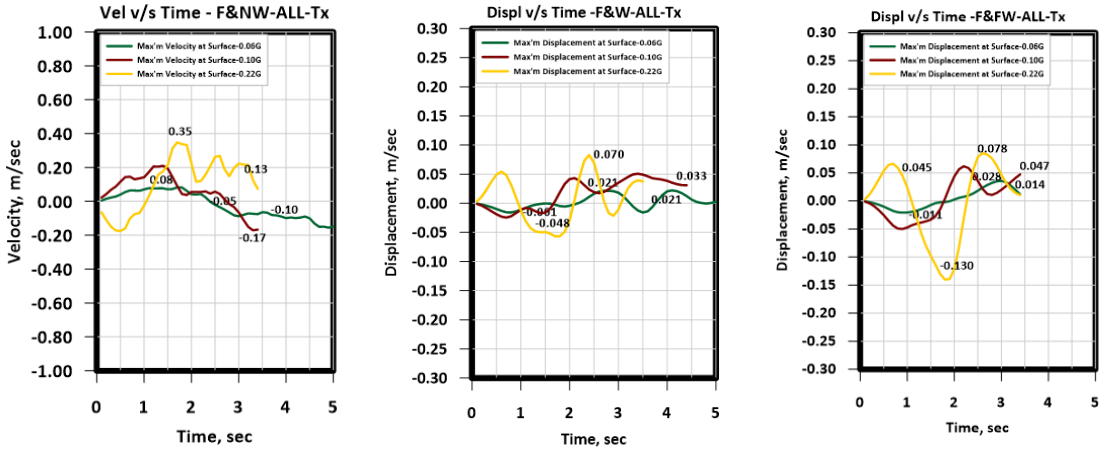

(a.) Fault & no water (b.) Fault & water (c.) Fault & full water

Figure 20. Velocity time history plot - at the ground surface for all three cases.

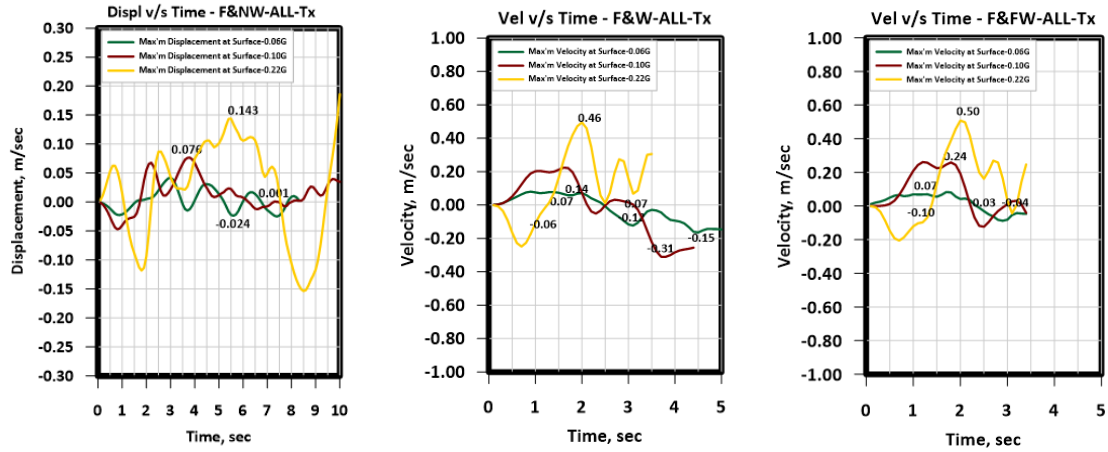

(a.) Fault & no water (b.) Fault & water (c.) Fault & full water

Figure 21. Displacement time plot - at the ground surface for all three cases.

Table 3. Maximum PGA, PGV & displacement values for Case 4 to Case 6 (cases with fault).

Sl. No.	Parameter	Seismic load applied					
		PGA = 0.06 g		PGA = 0.10g		PGA = 0.22 g	
		Horizontal	Vertical	Horizontal	Vertical	Horizontal	Vertical
Case 4: Fault & no water							
1	Peak Ground Acceleration (PGA), m/s^2	0.42	0.43	0.43	0.70	1.51	1.64
2	Peak Ground Velocity (PGV), m/s	0.08	0.09	0.21	0.07	0.34	0.38
3	Displacement (d), m	0.042	0.033	0.077	0.044	0.186	0.065
Case 5: Fault & water							
1	Peak Ground Acceleration (PGA), m/s^2	0.52	0.50	0.33	0.43	1.90	1.96
2	Peak Ground Velocity (PGV), m/s	0.08	0.09	0.22	0.17	0.49	0.25
3	Displacement (d), m	0.022	0.026	0.051	0.032	0.083	0.116
Case 6: Fault & full water							
1	Peak Ground Acceleration (PGA), m/s^2	0.29	0.30	0.27	1.23	1.48	1.06
2	Peak Ground Velocity (PGV), m/s	0.08	0.04	0.21	0.07	0.35	0.39
3	Displacement (d), m	0.036	0.015	0.062	0.018	0.085	0.150

Parametric numerical model studies were conducted for various scenarios, and the key observations are as follows:

1. The highest ground motions are observed in areas directly above the deepest excavated area (around Champion mine) in the central part of the mining region.
2. In most cases, the histories of vertical velocity surpass those of horizontal velocity.
3. The inundation of the mine significantly affects the intensity of the ground motions. As the water level transitions from a dry to a fully water-filled condition in the mine voids, there is a corresponding decrease in the intensity of ground motions.
4. The presence or absence of a fault plays a crucial role as it resembles a weak joint in a rock mass, greatly influencing ground motion parameters. The existence of a fault creates a vulnerable zone where the intensity of ground motions is higher compared to other areas.
5. Considering different scenarios with the presence of a fault and using the Mercalli Scale (USGS Instrumental Intensity Scale) for Peak Ground Acceleration and Velocity, the severity of seismicity (based on maximum values observed) can be categorized as shown in Table 4.

Table 4. The severity of the induced seismicity experienced on the surface.

Case condition	Instrumental intensity	Perceived shaking	Potential damage
Case: **PGA = 0.06 g**			
Fault & no water	V	Moderate	Very light
Fault & water	V	Moderate	Very light
Fault & full water	IV	Light	None
Case: **PGA = 0.10g**			
Fault & no water	V	Moderate	Very light
Fault & water	V	Moderate	Very light
Fault & full water	VI	Strong	Light
Case: **PGA = 0.22 g**			
Fault & no water	VI	Strong	Light
Fault & water	VII	Very Strong	Moderate
Fault & full water	VI	Strong	Light

6. Conclusions

The Midas GTS NX software tool, based on the Finite Element Method (FEM), was utilized to perform numerical simulations of seismic loads of different magnitudes. These simulations were executed under various scenarios, specifically: (i) dry conditions (ii) conditions with the actual water level (iii) conditions with water reaching the surface in the mine voids. Evaluating ground motions in the form of time histories offered a more accurate estimation of the potential seismic hazard that the mine could face under different seismic loads. The seismic loads applied were equivalent to the intensity of the maximum mining-induced seismicity experienced in the mine. This research work introduces a numerical modelling methodology for assessing the stability of a deep underground Kolar Gold

fields mine, which has a depth of 3.2 km under various seismic loading conditions.

The primary objective of this study was to examine the impact of the Mysore North fault that runs across the entire mining area under different loading conditions and to evaluate the post-mining induced seismicity and its effects on the surface above the mining area. Based on the results, a seismic hazard vulnerability map of the mining area was created for all simulated numerical model combinations. The results suggest that for a seismic load of PGA 0.22 g, for fault and actual water level combination, very strong shaking, and moderate potential surface damage were observed at vulnerable zones with a maximum PGA of 0.196 g and Peak Ground Velocity (PGV) of 0.49 m/s.

The closure of a mine and land reclamation is the final stage of a mining life cycle. If appropriate closure measures and reclamation policies are not implemented, the mine can become unsafe and unstable, leading to risks such as surface subsidence and sinkhole formations. Even after the complete closure of the Kolar Gold fields mine, post-mining induced seismic activities are still observed and recorded throughout the year. The ongoing presence of these post-mining induced seismic activities emphasizes the need to monitor these activities using a dedicated microseismic monitoring system with sensors placed at the most vulnerable zone locations assessed from the numerical modelling studies conducted. The suggested remedial measures for this underground mine include regular dewatering of mine workings based on water accumulation and backfilling of mine voids with suitable fill material. The excavated mine material could be recycled as fill material [62, 63]. The safety of structures and residences above the mining area should be prioritized. Once the mine stabilizes, land reclamation studies and rehabilitation studies can be initiated.

The use of finite element method software, specifically Midas GTS NX, in dynamic modelling methodology, has been recognized as a more reliable, feasible, efficient, and simple method for assessing the stability of closed mines. Minor instability within the mining area can cause hard and brittle rock mass to fail abruptly and transition from elastic to plastic zones. However, this transition from continuum to discontinuum after rock mass failure upon seismic load application could not be explored due to limitations in FEM software. Detailed post-failure studies on rock mass could be conducted using discrete element method software.

Acknowledgments

The authors express their gratitude to Dr. H S Venkatesh, Director of the National Institute of Rock Mechanics (NIRM), for granting permission to publish this research work. They also extend their appreciation to Dr. Sripad R Naik, Head of the Department of Numerical Modelling at NIRM, for his unwavering support and guidance. Furthermore, the authors would like to convey their thanks to Dr. V R Balasubramaniam, Project Leader of the Science and Technology research project in the study area, which was funded by the Ministry of Mines, Government of India.

References

[1]. Durrheim, R. J., Anderson, R. L., Cichowicz, A., Ebrahim-Trollope, R., Hubert, G., Kijko, A., McGarr, A., Ortlepp, W. D., & van der Merwe N. (2006). *The Risks to Miners, Mines and the Public posed by Large Seismic Events in the Gold Mining Districts of South Africa, Proceedings, of the Third International Seminar on Deep and High Stress Mining, Quebec City, Canada, 2-4 October*.

[2]. Simpson, D. (1986). Triggered earthquakes. *Ann. Rev. Earth Plan. Sci., 14*, 21-42.

[3]. Gupta, H.K. (1992). *Reservoir induced earthquakes. Volume 64*, *Elsevier*.

[4]. Deichmann, N., Kraft, T., & Evans, K. (2014). Mapping of faults activated by the stimulation of the Basel enhanced geothermal system. *Geothermics, 52*, 74-83.

[5]. McGarr, A., Simpson, D., & Seeber, L. (2002). Case histories of induced and triggered seismicity. *Academic Press. volume International Handbook of earthquake and engineering seismology of International Geophysics Series, chapter 40*, 647-661.

[6]. Davies, R., Foulger, G., Bindley, A., & Styles, P. (2013). Induced seismicity and hydraulic fracturing for the recovery of hydrocarbons. *Marine and Petroleum Geology, 45*, 171-185.

[7]. Gokhan, Kulekçi, Ali, Osman & Yilmaz (2019). Investigation of the Effect of Activities in Copper Mine on Historical Works. *Journal of underground resources, Year:8*, 16.

[8]. Martyna, Szydlowska (2016). Systematic review of Georisk in underground hard rock mines. *Master's Dissertation, European Mining, Minerals and Environmental Program, Aalto University*.

[9]. Gibowicz, S. J. (1990). Seismicity Induced by Mining. *Advances in Geophysics, vol. 32,* 1-74.

[10]. Boettcher, M. S., D. L. Kane, A. McGarr, M. J. Johnston, & Z. E. Reches (2015). Moment tensors and other source parameters of mining-induced earthquakes in TauTona Mine, South Africa. *Bull. Seismol. Soc. Am., 105*, 1576-1593.

[11]. Arora, S. K., Willy, Y. A., Srinivasan, C., & Benady, S. (2001). Local Seismicity due to Rockbursts and near-Field Attenuation of Ground Motion in the Kolar Gold Mining Region, India. *International Journal of Rock Mechanics and Mining Sciences, Vol. 38(5)*, 711-719.

[12]. Lizurek, G., Rudzinski, L., & Plesiewicz, B. (2015). Mining Induced Seismic Event on an Inactive Fault. *Acta Geophysica, 63(1)*, 176-200.

[13]. Orlecka-Sikora, B., Lasocki, S., Lizurek, G., & Rudziński, Ł. (2012). Response of seismic activity in mines to the stress changes due to mining induced strong seismic events. *International Journal of Rock Mechanics and Mining Sciences, 53*, 151-158.

[14]. Morissette, P. & Hadjigeorgiou, J. (2019). Ground support design for dynamic loading conditions: A quantitative data-driven approach based on rockburst case studies. *Journal of Rock Mechanics and Geotechnical Engineering*.

[15]. Larsson, K. (2004). Mining Induced Seismicity in Sweden. *Licentiate thesis, Lulea University of Technology*.

[16]. Li, T., Cai, M. F., & Cai, M. (2007). A review of mining-induced seismicity in China. International *Journal of Rock Mechanics and Mining Sciences, 44(8)*, 1149-1171.

[17]. Marty, Hudyma, Peter, Mikula & Michelle, Owen (2002). Seismic Hazard Mapping at Mt. Charlotte Mine. *Conference: Proceedings 6th North American Rock Mechanics Symposium Mining and Tunneling: Innovation and Opportunity at Toronto, Canada.*

[18]. Hudyma, M. R. (2008). Analysis and Interpretation of Clusters of Seismic Events in Mines. *Doctoral Dissertation, University of Western Australia*.

[19]. Hills, P.B., Mills, J., Penney, A.R., & Arthur, S. (2008). The development and implementation of a fully remote stoping method at Beaconsfield Gold Mine, Tasmania. *In Proceedings, of the Narrow Vein Mining Conference, The Australasian Institute of Mining and Metallurgy, Melbourne*, 199-206.

[20]. Varden, R. & Esterhuizen, H. (2012). Kanowna Belle – evolution of seismicity with increasing depth in an ageing mine. *In Y Potvin (ed.), Deep Mining 2012: Proceedings of the Sixth International Seminar on Deep and High Stress Mining, Australian Centre for Geomechanics, Perth*, 211-227.

[21]. Dineva, S. & Boskovic, M. (2017). Evolution of seismicity at Kiruna Mine. *Deep Mining 2017: Eighth International Conference on Deep and High Stress Mining - J Wesseloo (ed.) © 2017, Australian Centre for Geomechanics*, Perth.

[22]. Isabelle, Contrucci, Dalija, Namjesnik, Peter, Niemz, Paloma, Primo, Andrzej, Kotyrba, Grzegorz, Mutke, Petr, Konicek, Pascal, Dominique, Tobias, Rudolph, Stefan, Mollerherm, Jannes, Kinscher, Emmanuelle, Klein & Simone, Cesca (2023). European feedback on post-mining seismicity. *Journal of Sustainable Mining, 22*, 195-218.

[23]. Handley, M. F. (2013). Pre-mining stress model for subsurface excavations in Southern Africa. *Journal of the Southern African Institute of Mining and Metallurgy, Vol. 113(6)*, 449-471.

[24]. Joanna, Holmgren (2015). Induced Seismicity in the Dannemora Mine, Sweden. *Department of Earth Sciences, Uppsala University, Published at Department of Earth Sciences, Uppsala.*

[25]. Laura, Longoni, Monica, Papini, Davide, Brambilla, Diego, Arosio, & Luigi, Zanzi (2016). The risk of collapse in abandoned mine sites: the issue of data uncertainty. *Open Geosciences 2016, 8*, 246-258.

[26]. Emilio, Trigueros, Manuel, Canovas, Javier, Arzúa, & Manuel, Alcaraz (2021). Stability of an abandoned siderite mine: A case study in northern Spain. *Open Geosciences 2021, 13*, 359-376.

[27]. Geniş, M. & Aydan, O. (2020). Dynamic Analyses of Abandoned Mines During Earthquakes. *Environmental Geotechnics*, 1-12.

[28]. Ryder, J.A. (1988). Excess shear stress in the assessment of geologically hazardous situations. *J. South African Inst. Min. Metall., 88*, 27-39.

[29]. Spottiswoode, S.M. (1990). Volume excess shear stress and commutative seismic moments. *In:Fairhurst C (Editor) Rockbursts and Seismicity in Mines, Balkema, Rotterdam*, 39-49.

[30]. Hedley, D.G. F. (1992). Rockburst handbook for Ontario Hardrock mines. *CANMET Special Report SP92-1E*, 305.

[31]. Malovichko, D.A. (2017). Assessment and testing of seismic hazard for planned mining sequences. *Deep Mining 2017: Eighth International Conference on Deep and High Stress Mining - Wesseloo J (ed.) Australian Centre for Geomechanics*, Perth.

[32]. Poplawski, F.P. (1997). Seismicity underground with particular reference to rockburst problems at Mt. Charlotte mine. *Doctoral*

Dissertation, The University of Melbourne, Melbourne, 319.

[33]. Wiles, T.D. (1998). Correlation between Local Energy Release Density and Observed Bursting Conditions at Creighton Mine. *Mine Modelling Pty Ltd report, Mt Eliza, Australia*, 3930.

[34]. Beck, B.A. & Brady, B.H.G. (2002). Evaluation and application of controlling parameters for seismic events in hard-rock mines. *International Journal of Rock Mechanics and Mining Sciences, Vol. 39*, 633-642.

[35]. Bolt, B.A. & Abrahamson, N.A. (2003). Estimate of Strong Seismic Ground Motions. *In International Handbook of Earthquake and Engineering Seismology, IASPEI, Part B*.

[36]. Hudyma, M.R. (2004). Mining-induced seismicity in underground, mechanised, Hardrock mines-results of a World Wide Survey. *Australian Centre for Geomechanics, Research Report, Perth*.

[37]. Orlecka-Sikora, B., Papadimitriou, E. E., & Kwiatek, G. (2009). A study of the interaction among mining-induced seismic events in the Legnica-Głogów Copper District, Poland. *Acta Geophysica, 57(2)*, 413-434.

[38]. Sarfraz, Ali (2016). Evaluation of flooding induced mining seismicity with a view to characterize safety margins for surface structures under existing and flooded conditions in the Central Rand, Johannesburg. *Doctoral Dissertation, the Faculty of Engineering and the Built Environment, University of the Witwatersrand, Johannesburg*.

[39]. Brown, L. & Hudyma, M. (2017). Identifying local stress increase using a relative apparent stress ratio for populations of mining-induced seismic events. *Canadian Geotechnical Journal, 54(1)*, 128-137.

[40]. Kijko, A. (1997). Keynote lecture: Seismic hazard assessment in mines. *In Proc. 4th Int. Symp. on Rockbursts and Seismicity in Mines (eds. Gibowicz, S.J. and Lasocki, S.), Balkema, Rotterdam*, 247-256.

[41]. Lasocki, S. (2008). Some unique statistical properties of the seismic process in mines. *Proceedings of the 1st Southern Hemisphere International Rock Mechanics Symposium, (Editors: Potvin Y, Carter J, Dyskin A, and Jeffrey R) Perth, Australian Centre for Geomechanics, Vol. 1*, 667-678.

[42]. Ping, Wang, Ze, Zhao, Da, Zhang & Zeng, Chen (2023). Investigation of Microseismic Characteristics of Rock Burst Based on Fractal Theory. *Appl. Sci. 2023, 13*, 4613.

[43]. Changbin, Wang, Guangyao, Si, Chengguo, Zhang, Anye, Cao, Ismet, Canbulat (2023). Variation of seismicity using reinforced seismic data for coal burst risk assessment in underground mines. *International Journal of Rock Mechanics and Mining Sciences, Volume 165*, 105363.

[44]. Voza, A., Valguarnera, L., Marrazzo, R., Ascari, G., & Boldini, D. (2023). A new in-situ test for the Assessment of the Rock-Burst Alarm Threshold during Tunnelling. *Rock Mechanics and Rock Engineering, 56*, 1645-1661.

[45]. Meifeng, Cai (2015). Prediction and prevention of rockburst in metal mines: A case study of Sanshandao gold mine. *Journal of Rock Mechanics and Geotechnical Engineering*, 1-8.

[46]. Arciszewski, T. & Ziarko, W. (1992). Machine learning in knowledge acquisition. In: Arciszewski, T., Rossman, L.A. (Eds.), Knowledge acquisition in civil engineering. *American Society of Civil Engineers (ASCE)*, 50-68.

[47]. Michalski, R.S., Michalski, I., Bratko, I., & Kubat, M. (1998). *Machine learning and data mining: methods and applications, Wiley*.

[48]. Leu, S.S., Lo, H.C. (2004). Neural-network-based regression model of ground surface settlement induced by deep excavation. *Automation in Construction, 10*, 429-441.

[49]. Barkat, Ullah, Muhammad, Kamran, & Yichao, Rui (2022). Predictive Modeling of Short-Term Rockburst for the Stability of Subsurface Structures Using Machine Learning Approaches: t-SNE, K-Means Clustering and XGBoost. *Mathematics, 10*, 449.

[50]. Muhammad, Kamran (2021). A State-of-the-art Catboost-based T-Distributed Stochastic Neighbor Embedding Technique to Predict Back-break at Dewan Cement Limestone Quarry. *Journal of Mining and Environment, Vol. 12(3)*, 679-691.

[51]. Muhammad, Kamran, Ridho, Kresna, Wattimena, Danial, Jahed, Armaghani, Panagiotis, G., Asteris, Izhar, Mithal, Jiskani, & Edy, Tonnizam, Mohamad (2023). Intelligent based decision-making strategy to predict fire intensity in subsurface engineering environments. *Process Safety and Environmental Protection, 171*, 374-384.

[52]. Jing, L. (2003). A review of techniques, advances and outstanding issues in numerical modelling for rock mechanics and rock engineering. *International Journal of Rock Mechanics and Mining Sciences, 40(3)*, 283-353.

[53]. Alemdag, Selcuk, Zeybek, Halil, Ibrahim, Kulekci, Gokhan (2019). Stability evaluation of the Gumuşhane-Akçakale cave by numerical analysis method. *J. Mt. Sci., 16(9)*, 2150-2158.

[54]. Srinivasan, C., Benady, S., & Sivakumar, C. (2000). Fluid induced seismicity in Kolar Mining Region. *In: Proc. Workshop on Dam Safety*

Including Instrumentation of Dams, Trivandrum, November 15-17.

[55]. Srinivasan, C., Willy, Y.A., & Carter, R.M. (2013). Characteristics of Rockbursts in the flooded mines of Kolar Gold Field. *8th International Symposium on Rockbursts and Seismicity in Mines, Moscow, Russia*.

[56]. Praveena, Das, Jennifer, Balasubramanian, V.R., Goverdhan, K., & Ganapathy, G.P. (2016). Overview of seismic monitoring and assessment of seismic hazard based on a decade of seismic events. *Proc. of the International Conference on Recent Advances in Rock Engineering, Bengaluru, India, November 16-18*, 238-245.

[57]. Praveena, Das, Jennifer, Sripad, R., Naik, Porchelvan, P., & Harsha, Tadavarthi (2021). Stability analysis of an abandoned deep metal mine using numerical analysis tool: A case study. *ISRM regional conference -11th Asian Rock Mechanics Symposium (ARMS 11) China, IOP Conf. Series: Journal of Earth and Environmental Science Journal, 861(3)*, 032091.

[58]. Panduranga, R., Dharuman, R., Purusottaman, D., & Mishra, A.K. (2009). A Report on Geotechnical Evaluation of Rockburst Hazard in BGML area, Kolar Gold Fields, Kolar District, Karnataka. *Geological Survey of India, FS 2005-07*.

[59]. Hoek, E. & Brown, E.T. (2019). The Hoek–Brown failure criterion and GSI-2018 edition. *Journal of Rock Mechanics and Geotechnical Engineering, 11(3)*, 445-63.

[60]. Housner, G.W. & Jennings, P.C. (1964). Generation of artificial earthquakes. *Journal of the Engineering Mechanics Division (American Society of Civil Engineers), 90*, 113-150.

[61]. Srinivasan, C., Yesurathenam, Willy, & Gupta, Iswar (2010). Estimation of the local magnitude of rockbursts using strong motion accelerograms in the mines of Kolar Gold Fields. *Acta Geophysica, 58(2)*, 300-316.

[62]. Kulekci, G. & Ali, Yılmaz (2018). A case study on the effects of stone quarries on environment and agricultural land. *Bahce 47*, 230-237.

[63]. Kulekci, G., Ali, Yılmaz & Cullu, M. (2021). Experimental investigation of the usability of construction waste as aggregate. *Journal of Mining and Environment, 12 (1)*, 63-76.

تحلیل اجزای محدود خطر لرزه‌ای در محیط‌های پس از معدنکاری معادن سنگ سخت زیرزمینی بسته شده

پراوینا داس جنیفر[۱] و پورچلوان پی.[۲*]

۱ .مرکز کاهش بلایا و مدیریت(CDMM) ، موسسه فناوری ولور، ولور ، تامیل نادو، هند

۲. دانشکده مهندسی عمران (SCE)، موسسه فناوری ولور ، ولور ، تامیل نادو، هند

ارسال ۲۰۲۳/۰۸/۰۵، پذیرش ۲۰۲۳/۱۱/۰۷

* نویسنده مسئول مکاتبات: pporchelvan@vit.ac.in

چکیده:

این مقاله یک مطالعه جامع در مورد پایداری معدن طلای کولار (عمق ۳.۲ کیلومتر) تحت شـــرایط بارگذاری لرزه‌ای مختلف ارائه می‌کند. این مطالعه از ابزار نرم‌افزاری Midas GTS NX مبتنی بر روش المان محدود (FEM) برای انجام شبیه‌سازی عددی بارهای لرزه‌ای با شدت‌های مختلف تحت شرایط متعدد سطح آب در حفره‌های معدن اســتفاده کرد. بارهای لرزه‌ای اعمال شــده معادل شــدت حداکثر لرزه خیزی ناشــی از معدنکاری تجربه شــده در معدن بود. این مطالعه همچنین تأثیر گسل شمالی میسور و اثرات آن را بر سطح بالای منطقه معدن بررسی کرد. نقشه آسیب‌پذیری خطر لرزه‌ای منطقه معدن بر اساس نتایج برای همه ترکیب‌های مدل عددی شبیه‌سازی‌شده ایجاد شد. نتایج استنباط کردند که برای بار لرزه‌ای PGA، ۰.۲۲ گرم، برای ترکیب گسل و سطح آب واقعی، لرزش بسیار قوی و آسـیب سـطحی بالقوه متوسـط در مناطق آسـیب‌پذیر با حداکثر PGA 0.196 گرم و حداکثر سـرعت زمین (PGV) مشـاهده شـد. ۰.۴۹ متر بر ثانیه این مطالعه اهمیت نظارت بر فعالیت‌های لرزه‌ای ناشی از پس از معدن را با استفاده از یک سیستم پایش ریز لرزه‌ای اختصاصی با سنسورهایی که در آسیب‌پذیرترین مکان‌های منطقه ارزیابی شده از مطالعات مدل‌سازی عددی انجام‌شده قرار داده شده‌اند، برجسته می‌کند. اقدامات اصلاحی پیشنهادی شامل آبگیری منظم عملیات معدن بر اسـاس انباشـت آب و پرکردن فضـای خالی معدن با مواد پرکننده مناسـب اسـت. رویکرد مدل‌سـازی پویا با اسـتفاده از Midas GTS NX روشـی قابل اعتمادتر، امکان‌پذیر، کارآمد و ساده‌تر برای ارزیابی پایداری معادن بسته است.

کلمات کلیدی: روش المان محدود، بسته شدن معدن، لرزه خیزی القایی، مطالعات مدلسازی، مدلسازی دینامیکی.